Composites Part C: Open Access 6 (2021) 100184

Contents lists available at ScienceDirect

Composites Part C: Open Access

journal homepage: www.sciencedirect.com/journal/composites-part-c-open-access

Elastic properties of heterodesmic composite structures: The case of calcite $CaCO_3$ (space group $R\bar{3}c$)

Gianfranco Ulian *, Daniele Moro, Giovanni Valdrè *

Centro di Ricerca Interdisciplinare di Biomineralogia, Cristallografia e Biomateriali, Dipartimento di Scienze Biologiche, Geologiche e Ambientali, Università di Bologna "Alma Mater Studiorum", Piazza di Porta San Donato 1, 40126 Bologna, Italy

ARTICLE INFO

Keywords:
Calcite
Elastic constants
Equation of state
Density Functional Theory
DFT
van der Waals interactions

ABSTRACT

Composite-like structures are commonly found in nature and, among them, calcite ($CaCO_3$, space group $R\bar{3}c$) is made of alternately stacked layers of Ca^{2+} and triangular CO_3^{2-} ions. The bonding scheme of this mineral results in an heterodesmic structure because the carbonate ions are made up of covalent bonds (acting along the crystallographic **a-** and **b**-axes) and the positive Ca^{2+} and negative CO_3^{2-} layers are held together by electrostatic interactions (along the **c**-axis). Because of its structure and heterodesmic nature, calcite is a highly anisotropic material suitable as a test case to design, develop and assess the quality of theoretical approaches to model composite-like structures. In the present work, the structural and elastic properties (second-order elastic constants and equation of state) of calcite have been investigated by means of the Density Functional Theory, comparing several Hamiltonians and specific *a posteriori* corrections to treat the weak long-range interactions. Both second-order elastic moduli and the equation of state of calcite were obtained and discussed in comparison to well-established experimental data. The results and the approach presented in this *in silico* work could be of use for the characterization of elastic properties of other similar minerals/crystal structures used in composites for structural applications.

1. Introduction

In crystal-chemistry, heterodesmic structures are crystalline materials whose atoms are bonded together in more than a single way, *i.e.*, they exhibit a mix covalent, ionic, and/or weak long-range interactions (such as hydrogen bonds and van der Waals ones). Well-known examples of this kind of materials are natural graphite (C) and synthetic hexagonal boron nitride (hBN), where the atoms are strongly bonded by covalent bonds, forming bi-dimensional layers that are held together by weak dispersive forces [1]. Other natural heterodesmic crystals are, for example, portlandite $Ca(OH)_2$, molybdenite MoS_2, phyllosilicates (*e.g.*, smectite, pyrophyllite, talc, etc.), all presenting a layered structure with strong in-plane bonds and weak out-of-plane interactions [2,3]. Typical characteristics of the materials cited above are the high anisotropy in all tensorial physical properties (*e.g.*, stiffness), the easy cleavage in single- or multi-layers and the possibility to create heterostructures (composites) by stacking layers of different materials, such as, to cite an example, graphene and MoS_2 [4].

Among the different heterodesmic crystals, calcite, the mineralogical name of calcium carbonate ($CaCO_3$, trigonal system, space group $R\bar{3}c$, Fig. 1) presents a mix of covalent C–O bonds within the carbonate groups and electrostatic (ionic) Ca^{2+} ••• CO_3^{2-} interactions. In addition, this mineral crystallizes with a composite-like structure, with alternated layers of negatively charged carbonate ions held together by layers of calcium cations, where each Ca^{2+} ion octahedrally coordinates six oxygen atoms from six different CO_3^{2-} groups (see Fig. 1). Calcite is an ubiquitous mineral on the Earth's crust, commonly found in both sedimentary rocks (*e.g.*, limestone, marl) and metamorphic ones (marbles), with several uses in technological applications. For example, calcite and calcite-bearing rocks have been employed since the ancient times to realize buildings and construction materials, as documented in several archaeological reports [5–8]. Furthermore, in modern times, calcite represents the main source of lime (CaO, calcium oxide) for the production of Portland cement, which is produced by sintering limestone and clay (aluminosilicates), or marls with appropriate $CaO:SiO_2:Al_2O_3$ ratios [9–11].

Given the utmost importance of this heterodesmic mineral in building and construction materials, it was the subject of several

* Corresponding authors.
E-mail address: giovanni.valdre@unibo.it (G. Valdrè).

https://doi.org/10.1016/j.jcomc.2021.100184
Received 10 August 2021; Accepted 11 August 2021
Available online 15 August 2021

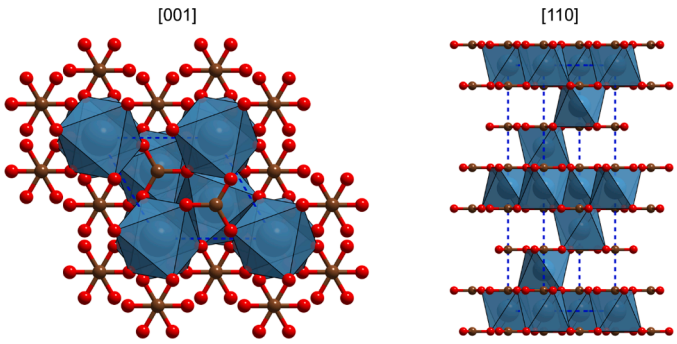

Fig. 1. Crystal structure of calcite, in its trigonal representation, as seen from the [001] and [110] directions. The dashed blue line is the crystal lattice. Oxygen and carbon atoms are coloured in red and ochre, respectively. The octahedral coordination of calcium ions is represented by the dark cyan polyhedral.

experimental works devoted to the investigation of its important anisotropic properties, in particular its mechanical behaviour [12–15]. Also, since its structure is relatively simple (crystallographic trigonal cell with six formula units, $Z = 6$, primitive rhombohedral cell with $Z = 2$), it represents a suitable model to test the accuracy of different theoretical methods in describing the physical and chemical properties of heterodesmic crystals. For example, Valenzano and co-workers [16] performed a comparison between different Density Functional Theory (DFT) approaches for the characterization of structural, dielectric and vibrational properties. However, a similar comparison considering the elastic properties (stiffness and behaviour under hydrostatic compression) of calcite is still missing in literature. There are different theoretical works that provided mechanical data on this mineral phase, but they were carried out with too different computational setups (theoretical frameworks, computer codes, convergence criteria, and so on), which hinder a thoughtful comparison and fruitful discussion [17,18].

In this context, the present paper is intended to fill this knowledge gap, providing for the first time an accurate and detailed comparison between the performance of different DFT methods in describing the mechanical behaviour of calcite. Six DFT functionals were carefully selected, considering their known accuracies in describing structural, chemical and physical properties [19,20]. In addition, the effects of different *a posteriori* schemes for the inclusion of long-range interactions are also compared, considering a total of 14 combinations of Hamiltonians and van der Waals corrections. This implementation is extremely important for calcite because of the heterodesmic nature and is here proposed and discussed in relation to the elastic properties. Some of these combinations of functionals/corrections were recently employed to describe the structural, dielectric, optical and vibrational properties of calcite [21], but not the elastic ones, which will be the topic of the present paper.

2. Computational methods

2.1. Hamiltonian and computational parameters

The results of the present work were obtained through ab initio simulations carried out with the CRYSTAL17 code, employing the Kohn–Sham self-consistent field (SCF) method [22].

The choice of the DFT Hamiltonian considered the first four rungs of the Jacob's ladder depicted by Perdew and collaborators [23]. In detail, the first and second rungs of the cited ladder are given by the local-density approximation (LDA) and by the generalized-gradient approximation (GGA, or semilocal) functionals, respectively. There are several GGA formulations, and the one proposed by Perdew-Burke-Ernzerhof (PBE) was here employed [24]. The third rung is given by meta-GGA Hamiltonians, from which the M06L developed by Zhao and Truhlar [25] was the one selected. For the sake of clarity, LDA is the simplest approximation, where the exchange and correlation total energy depends only on the electron density of the system under analysis, whereas GGA and meta-GGA approaches include the first derivative (gradient) and second derivative (Laplacian) of the electronic density, respectively. The fourth rung of the Jacob's ladder is represented by hybrid functionals, which include a fraction of exact Hartree-Fock (HF) exchange. In the present work, three most used formulations (in parentheses the HF fraction) were adopted, *i.e.,* PBE0 (25%), B3LYP (20%) [26,27] and M06 (27%) [25].

The integration grid over which the total energy was calculated is the default one provided by CRYSTAL17, which is a pruned grid with 75 radial points and a maximum number of 974 angular points in regions relevant for chemical bonding, subdivided in five shells with different angular grids (XLGRID keyword) [22]. The numerical accuracy for the calculation of the Coulomb and exchange integrals was set to ITOL1 = 8, ITOL2 = 8, ITOL3 = 8, ITOL4 = 8, ITOL5 = 16 [22]. The diagonalization of the Hamiltonian matrix was performed with a 6 × 6 × 6 Monkhorst-Pack [28] grid of k points in the reciprocal space.

The atomic basis sets employed in the construction of the multielectronic wave function are Gaussian-type orbitals, which are linearly combined to form crystalline orbitals. Calcium, oxygen and carbon were described by 8-6511(21), 8-411(11) and 6-311(11) basis sets, respectively, which were optimized by Valenzano et al. [16,29].

2.2. Inclusion of long-range interactions

Dispersive interactions are not properly described with standard GGA and hybrid DFT functionals, because of the exponential decay of the long-range correlation for semilocal Hamiltonians, which stems only from the region of electron density overlap [30,31]. In fact, the van der Waals interactions have a decay given by R^{-6}, with R the (usually large) distance between the objects (atoms, molecules, etc.), which explains why most of DFT functionals are not able to describe long-range interactions [32]. Obviously, this missing term severely affects the characterization of both the structure and elasticity of materials, including also many other properties (*e.g.*, thermodynamics, phonon dispersion relations). A successful approach to solve this limitation is given by the DFT-D*n* methods proposed by Grimme and co-workers [33,34], with n = 2 or 3. The DFT-D2 and DFT-D3 schemes are *a posteriori* corrections that add a van der Waals energy term (E_{Dn}) to the exchange-correlation energy (E_{DFT}), resulting in the total energy of the system $E_{TOT} = E_{DFT} + E_{Dn}$.

The DFT-D2 energy term (E_{D2}) is given by the following formula:

$$E_{D2} = -\frac{1}{2}\sum_{i=1}^{N}\sum_{j=1}^{N}\sum_{\mathbf{g}}\frac{C_{6ij}}{r_{ij,\mathbf{g}}^{6}} f_{dump,6}\left(r_{ij,\mathbf{g}}\right),$$

whereas the DFT-D3 correction (E_{D3}) is expressed as:

$$E_{D3} = -\frac{1}{2}\sum_{i=1}^{N}\sum_{j=1}^{N}\sum_{\mathbf{g}}\left[\frac{C_{6ij}}{r_{ij,\mathbf{g}}^{6}} f_{dump,6}\left(r_{ij,\mathbf{g}}\right) + \frac{C_{8ij}}{r_{ij,\mathbf{g}}^{8}} f_{dump,8}\left(r_{ij,\mathbf{g}}\right)\right].$$

The summations in the above formulas are performed over the number of atoms N, where $r_{ij,\mathbf{g}}$ represents the internuclear distance between atom i in cell $\mathbf{g} = 0$ (reference cell) and atom j in cell $\mathbf{g}$, C_{6ij} and C_{8ij} are the nth-order dispersion coefficients for atom pairs ij. The long-range energy is damped by the function $f_{dump,n}(r_{ij,\mathbf{g}})$, so the weak van der Waals interactions do not contribute to other kind of bonds (*e.g.*, ionic, covalent) typically found at short distances. For the DFT-D2 approach, the damping function is expresses as:

$$f_{dump,6}\left(r_{ij,\mathbf{g}}\right) = s_6\left[1 + e^{-d\left(r_{ij,\mathbf{g}}/R_{vdW}-1\right)}\right]^{-1}$$

with s_6 a scaling parameter that varies according to the adopted functional (e.g., for PBE it is 0.75), R_{vdW} the sum of van der Waals radii of

atoms *i* and *j* and *d* the steepness of the damping (set to 20 in the present work). The C_{6ij} parameters are calculated as a geometrical mean:

$$C_{6ij} = \sqrt{C_{6i}C_{6j}}$$

where C_{6i} and C_{6j} are tabulated for each atom and kept fixed during the simulation [33].

The DFT-D3 scheme is less empirical than the DFT-D2, because the C_{nij} ($n = 6, 8$) parameters are dependent on the geometry of the system, and not fixed. Another difference between the two schemes is given by the damping function, which may have different formulations. Here it was employed the one of Becke and Johnson [35–37]:

$$f_{dump,n}(r_{ij,\mathrm{g}}) = \frac{s_n r_{ij}^n}{r_{ij}^n + f(R_{0ij})^n}$$

where $R_{0ij} = \sqrt{C_{8ij}/C_{6ij}}$ and $f(R_{0ij}) = \alpha_1 R_{0ij} + \alpha_2$. In this formulation, $s_6 = 1$, s_8, α_1 and α_2 are adjustable parameters. It is worth highlighting that (i) there is not any DFT-D*n* parametrization for LDA functional and (ii) only the DFT-D3 scheme is available for the M06L (meta-GGA) and M06 (hybrid) functionals.

2.3. Geometry optimization and calculation of elastic properties

The optimization of the calcite geometry was performed by simultaneously varying lattice parameters and atomic coordinates, using an analytical gradient method for the latter and a numerical gradient for the unit cell parameters. The convergence criterium for geometry optimization was set to 10^{-5} hartree bohr^{-1} for the gradient and to $4 \cdot 10^{-5}$ bohr for the maximum atomic displacement, with respect to the previous optimization step.

The elastic constants are the elements of the fourth-rank tensor **C** (called also 'stiffness' tensor), which are defined as:

$$\sigma_{ij} = C_{ijkl}\eta_{kl}$$

where σ_{ij} and η_{kl} are the components of the stress and pure strain second-rank tensors, respectively. In this notation, *i, j, k, l* = *x, y, z* are Cartesian directions. By using the Voigt's notation, it is possible to express the fourth rank tensor **C** as a 6 × 6 matrix whose elements are identified by the indexes *v,u* = 1, …, 6, where 1 = *xx*, 2 = *yy*, 3 = *zz*, 4 = *yz*, 5 = *xz* and 6 = *xy* [38]. Hence, the previous equation can be rewritten as:

$$\sigma_v = C_{vu}\eta_u$$

The elements C_{vu} are also defined as the second derivative of the lattice energy with respect to the applied strain:

$$C_{vu} = \left.\frac{\partial^2 E}{\partial\eta_v \partial\eta_u}\right|_0$$

where 0 indicates the stiffness is calculated at the equilibrium geometry. Calcite belongs to the crystal class $\bar{3}m$, hence it presents 6 independent elastic constants and the stiffness matrix in Voigt notation is then:

$$\begin{pmatrix} C_{11} & C_{12} & C_{13} & -C_{14} & \cdot & \cdot \\ & C_{11} & C_{13} & C_{14} & \cdot & \cdot \\ & & C_{33} & \cdot & \cdot & \cdot \\ & & & C_{44} & \cdot & \cdot \\ & & & & C_{44} & \cdot \\ & & & & & C_{66} \end{pmatrix}$$

where $C_{66} = (C_{11} - C_{12})/2$. The compliance matrix **S** is calculated as the inverse of the stiffness one, $\mathbf{S} = \mathbf{C}^{-1}$. The elastic moduli were calculated by a fully automated procedure provided by the CRYSTAL code, using 5 points of displacement for each necessary lattice deformation, with a step of 0.005 Å. The interested readers can find more insights of the automated procedure in the works of Perger and co-workers [39,40]. The crystallographic axes of calcite were oriented according to the standards of the Institute of Radio Engineering, *i.e.*, the crystallographic **a**-axis and **c**-axis were parallel to the –*x* and *z* directions, respectively [41]. Single-crystal elastic properties, namely Young's modulus (E), linear compressibility (β), shear modulus (μ) and Poisson's ratio (υ) were calculated from the elastic moduli using a development version of the Quantas code [42], using well-known directional relations [38,43–45].

Voigt and Reuss equations were employed to calculate the upper and lower bounds of bulk modulus (upper = K_V; lower = K_R) and shear modulus (upper = μ_V; lower = μ_R), considering the system as a poly-crystalline aggregate as explained by Nye [38]:

$$K_V = \frac{[C_{11} + C_{22} + C_{33} + 2(C_{12} + C_{13} + C_{23})]}{9}$$

$$K_R = [S_{11} + S_{22} + S_{33} + 2(S_{12} + S_{13} + S_{23})]^{-1}$$

$$\mu_V = \frac{C_{11} + C_{22} + C_{33} + 3(C_{44} + C_{55} + C_{66}) - (C_{12} + C_{13} + C_{23})}{15}$$

$$\mu_R = \frac{15}{4}[S_{11} + S_{22} + S_{33} + 3(S_{44} + S_{55} + S_{66}) - (S_{12} + S_{13} + S_{23})]^{-1}$$

According to the Voigt-Reuss-Hill (VRH) method [46], it is possible defining the means of the bulk and shear moduli as:

$$K_{VRH} = \frac{1}{2}(K_V + K_R) \text{ and } \mu_{VRH} = \frac{1}{2}(\mu_V + \mu_R)$$

The Young's modulus, E, and the Poisson's ratio, υ, are then given by: $E = \frac{9K\mu}{3K+\mu}$ and $\upsilon = \frac{3K-2\mu}{2(3K-\mu)}$ where it is possible using either the Voigt, Reuss and the Voigt-Reuss-Hill values.

3. Results and discussion

3.1. Calcite crystal structure

Table 1 reports calcite structural data obtained from the geometry optimization, including the experimental XRD refinements performed

Table 1.
Lattice parameters *a* and *c*, unit cell volume *V*, *c*/*a* ratio, C – O and Ca — O distances (d_{C-O} and d_{Ca-O}, respectively) calculated with different DFT approaches and compared with X-ray diffraction results.

Method	*a* (Å)	*c* (Å)	*V* (Å^3)	*c*/*a*	d_{C-O} (Å)	d_{Ca-O} (Å)
LDA[a]	4.957	16.490	350.86	3.327	1.2834	2.3159
PBE[b]	5.045	17.313	381.67	3.432	1.2976	2.3882
PBE-D2[b]	5.020	16.955	370.08	3.377	1.2952	2.3607
PBE-D3[b]	5.026	17.034	372.64	3.389	1.2958	2.3668
M06L[a]	4.999	17.059	369.23	3.412	1.2865	2.3612
M06L-D3[a]	4.996	17.019	367.93	3.406	1.2862	2.3581
B3LYP[b]	5.041	17.320	381.08	3.436	1.2879	2.3915
B3LYP-D*[b]	5.028	16.968	371.52	3.375	1.2860	2.3695
B3LYP-D3[b]	5.007	16.822	365.17	3.360	1.2846	2.3535
PBE0[b]	5.007	17.215	373.73	3.438	1.2824	2.3745
PBE0-D2[b]	4.984	16.849	362.42	3.381	1.2801	2.3472
PBE0-D3[b]	4.988	16.932	364.85	3.395	1.2806	2.3530
M06[a]	4.985	16.973	365.30	3.405	1.2803	2.3540
M06-D3[a]	4.979	16.940	363.63	3.402	1.2798	2.3498
XRD[c]	4.991 (2)	17.062 (2)	368.1(3)	3.419 (2)	1.284 (1)	2.3590 (8)
XRD[d]	4.9891 (3)	17.0610 (7)	367.787 (4)	3.420	-	-

[a] – present work;
[b] – Ref. [21];
[c] – Ref. [47];
[d] – Ref. [15].

by different authors [15,47]. Some of the theoretical results, *i.e.*, those obtained with the PBE, B3LYP and PBE0 functionals were calculated and presented in a previous theoretical work [21], and they were here included both to extend the discussion on the *ab initio* determination of the calcite structure and because they are the starting point for the subsequent analysis of the elastic properties (*vide infra*).

Let the comparison between the different DFT approaches begin from the functionals not corrected for long-range interactions, using the calcite XRD refinement carried out by Maslen and co-workers [47] as a reference. For the sake of clearness, the theoretical results are obtained at absolute zero (0 K), whereas the experimental data were collected at room temperature (ca. 300 K). Possible thermal effects on the lattice geometry and atomic positions were not considered in the present work, hence the DFT simulations are considered "good" when the unit cell is smaller (to certain extent) than that experimentally determined. LDA resulted in a unit cell that is much smaller than that obtained from X-ray diffraction (about –5%), which is expected because local density approximation assumes that the electron density can be treated as a uniform electron gas. Consequently, LDA underestimates the exchange energy term and overestimates the correlation one, which leads to an overbinding effect (*e.g.*, very short Ca — O distances, see Table 1). Another expected result is the larger unit cell parameters (volume increase of about +4%) obtained from the PBE functional, which includes the gradient of the electron density, because of its well-known underbinding behaviour. The inclusion of the Laplacian (second derivative) of the electron density in the M06L meta-GGA functional provided a very good agreement between the theoretical unit cell of calcite and the experimental one, with a small overestimation of the volume (+0.3%). In general, the inclusion of some fraction of exact Hartree-Fock exchange in the hybrid functionals leads to an increased ionicity of the system (*i.e.*, increased electrostatic interactions), and in the PBE0 case it can be noted a remarkable improvement in the determination of the lattice volume (+1.5%) with respect to the standard PBE functional. The B3LYP Hamiltonian resulted in a slightly overestimated large unit cell (+3.5%), whereas the hybrid M06 shows some contraction of the volume because of the increased electrostatic interactions (–0.2%).

From the analysis of the atomic distances, it can be noted that the covalent C – O bonds is well described by all the chosen DFT functionals, with maximum and minimum absolute variations of about +1.1% (PBE) and –0.1% (LDA), respectively. The other functionals resulted in differences of about ±0.3% with respect to the experimental XRD data. As explained in the Introduction section, the main reason behind the overestimation of the unit cell volume resides in the Ca — O distances, which are severely overestimated by PBE (1.2%), B3LYP (+1.4%) and PBE0 (+0.7%), and highly underestimated by LDA (–1.8%). Instead, the meta-GGA functional M06L and its hybrid formulation M06 performed much better, with maximum absolute difference of 0.2%. It is interesting noting that the inclusion of a fraction of Hartree-Fock exchange in the PBE0 and M06 functionals resulted in smaller C – O and Ca — O distances with respect to the non-hybrid PBE and M06L approaches, in agreement with previous observations for other ionic structures [16,48,49]. However, the present simulations show that the use hybrid functionals is not sufficient to properly treat this heterodesmic structure, and the inclusion of dispersive forces in the physical description of calcite should be considered.

In fact, the DFT-D2 scheme, applied to the PBE, B3LYP and PBE0 functionals, led to a great improvement on the characterization of the calcite crystal structure, resulting in unit cell volumes that are +0.5%, +0.9% and –1.5% with respect to the XRD refinement [47]. In comparison with the uncorrected functionals, this *a posteriori* correction lowered the volume by about –3%. The C – O bond lengths are +0.9%, +0.2% and –0.3% and the Ca — O electrostatic interaction distances are +0.1%, +0.5% and –0.5% compared to the experimental findings of Maslen et al. [47], when simulated with the PBE-D2, B3LYP-D* and PBE0-D2 approaches, respectively.

The less empirical DFT-D3 correction was applied to all selected DFT functionals but the LDA one. Within the PBE-based Hamiltonians (generalized gradient approximation PBE and hybrid PBE0), it can still be noted the contraction of the unit cell volume, *i.e.*, an increase in the atomic interactions, but to a lesser extent with respect to that obtained from the DFT-D2 approach. Instead, the cell volume of calcite calculated from the B3LYP-D3 approach is about 2% lower than that obtained from B3LYP-D*, hence underestimated by about –0.8% with respect to the XRD results. This apparently discordant behaviour depends on the use of rescaled DFT-D2 parameters in the B3LYP-D* approach, as described by Civalleri and collaborators [50]. In fact, the authors of the cited work noticed that the standard B3LYP-D2 method produced much contracted unit cell volumes for several molecular crystals, other heterodesmic structures characterized by covalent intramolecular bonds and long-range intermolecular interactions. For this reason, they modified the atomic van der Waals radii entering in the damping function *f* (see Section 2.2) to make it active in a more long-range region, hence decreasing the dispersion contribution [50]. The same overbinding effect of B3LYP-D2 was observed in a theoretical work on talc, whereas more reliable results were calculated with the reparametrized B3LYP-D* approach [51], which was also applied to the simulations of other minerals presenting heterodesmic structures such as clinochlore [45] and portlandite [3].

While the DFT-D3 correction resulted in a considerable shrink of the calcite unit cell volume (about –2.4% for PBE and PBE0 and –4.2% for B3LYP), when applied to the meta-GGA functional M06L and its hybrid formulation M06 produced only a slight contraction of about –0.4% and –0.5%, respectively, when compared to the uncorrected DFT functionals. This suggests that the M60L and M06 functionals not corrected via the DFT-D3 scheme were already able to describe most of the mid-range and long-range interactions, in particular the non-covalent Ca — O ones. Indeed, the van der Waals correction reduced this distance by about –0.1% and –0.2% with M06L-D3 and M06-D3, respectively, and negligible variations were observed for the C – O covalent bonds (–0.02% and –0.04%, respectively).

3.2. Elastic properties

3.2.1. Elastic constants

The calculated second-order elastic constants calculated with the different combination of DFT approaches are reported in Table 2, alongside previous experimental [12,52] and theoretical results [17,53]. Fig. 2 instead shows as a bar plot the relative difference between the simulated stiffness and the experimental one of Chen and collaborators

Table 2.
Second-order elastic moduli (in GPa) calculated at DFT level with different computational approaches, compared to previous theoretical and experimental data reported in literature.

Method	C_{11}	C_{33}	C_{12}	C_{13}	C_{14}	C_{44}	C_{66}
LDA	179.77	93.25	79.55	72.74	-24.28	40.20	50.11
PBE	149.40	85.38	58.89	55.38	-16.37	32.59	45.26
PBE-D2	161.47	84.01	66.09	59.75	-20.79	35.64	47.69
PBE-D3	158.90	87.76	64.65	60.75	-18.98	34.83	47.13
M06L	171.24	90.91	78.89	66.78	-24.61	37.72	46.17
M06L-D3	171.42	90.68	79.39	67.02	-24.66	37.95	46.02
B3LYP	156.08	88.95	58.54	55.59	-17.90	35.22	48.77
B3LYP-D*	162.86	89.65	63.58	60.23	-20.67	36.64	49.64
B3LYP-D3	175.36	92.06	67.44	65.99	-23.04	39.96	53.96
PBE0	159.23	90.38	62.19	58.42	-18.81	35.88	48.52
PBE0-D2	171.76	88.23	69.87	63.61	-24.04	39.35	50.94
PBE0-D3	168.58	92.39	67.73	64.06	-21.74	38.20	50.42
M06	191.92	105.49	77.36	70.96	-22.56	38.21	57.28
M06-D3	194.04	106.62	79.09	72.46	-23.36	38.64	57.48
Exp. [12]	149.4	85.2	57.9	53.5	-20.0	34.1	45.8
Exp. [52]	144	84	53.9	51.1	-20.5	33.5	45.1
PBE [53]	143.5	69.8	43.9	41.7	0	34.9	49.8
FF [17]	153	82	55	50	-13	37	49

Notes: FF means simulations performed with force field (classical mechanics).

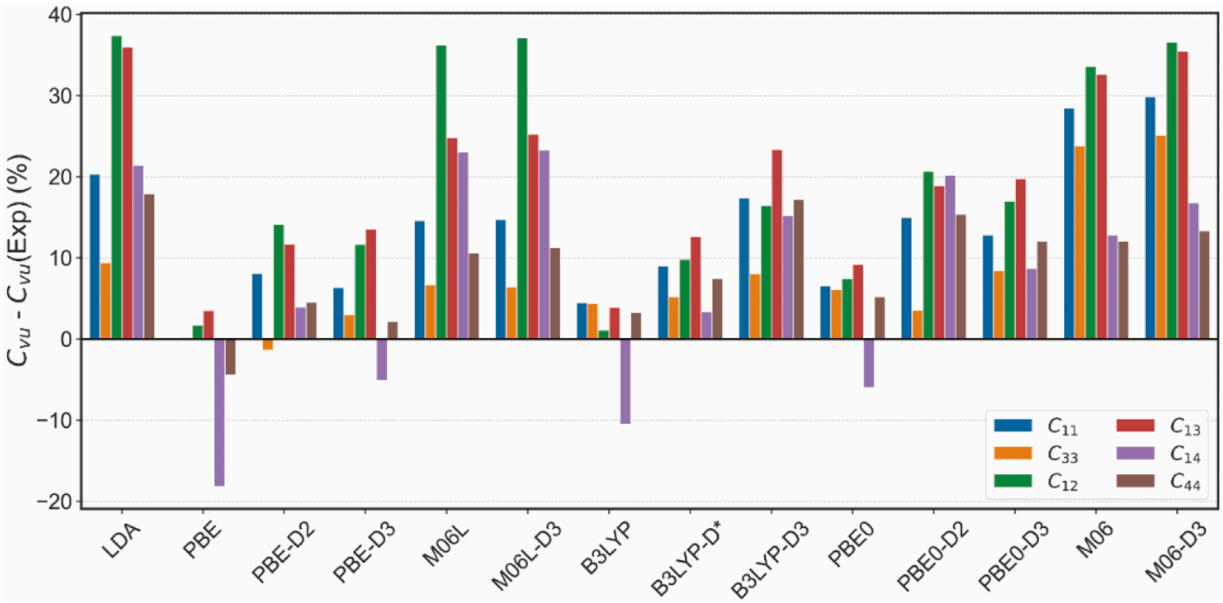

Fig. 2.. Relative differences (in %) between the elastic moduli calculated with different Density Functional Theory approaches and the experimental C_{vu} values of Chen and co-workers [12].

[12]. Polycrystalline averages, namely the values of the bulk (K), shear (μ) and Young's (E) moduli and the Poisson's ratio (υ) calculated assuming the material being made of randomly-oriented crystals, are reported in Tables 3 and 4.

In general, the results of the present work are in satisfactory agreement with those found in literature, but the Density Functional Theory data are always overestimated. Indeed, special care must be paid when discussing the similarities and differences between the different datasets. There are two main sources of discrepancy between the theoretical results and the experimental ones. The first one arises from both the Hellmann-Feynman theorem and the use of atom-centred Gaussian-type orbital basis sets, which are strictly dependent on the position of the nuclei. Within this framework, and because of the basis sets are incomplete, it is well-known that a small deviation occurs in the evaluation of the stress tensor during self-consistent field calculations, which is called Pulay stress (or Pulay forces), the derivative of the basis set with respect to the atomic position [54]. At present, this term is not considered by the CRYSTAL code, hence the elastic moduli are affected by this effect. In other works, it was shown that non-local basis sets, such as plane waves, reduce the Pulay forces effect, hence, the elastic constants are generally more accurately determined [55]. However, the error with the GTO basis sets is mitigated by increasing the number of Gaussian-type functions, asymptotically reaching a null value when the basis sets is complete.

The second discrepancy was introduced when discussing the crystal structure of calcite, namely the absence of thermal effects in the calculation of the second-order elastic constants. Hence, the simulated data are slightly stiffer because they were obtained at absolute zero (0 K), whereas the experimental elastic moduli were measured at room temperature (298 K). The authors are aware that there are at least two approximated methods that could improve the comparison with the experimental data, *i.e.*, the quasi-harmonic approximation and the quasi-static approximation, which were recently discussed by Destefanis and co-workers [56]. The interested reader may find more details on these formulations in the cited paper, it is sufficient noting that both methods are computational demanding, with the quasi-static

Table 3.
Bulk (K, in GPa), shear (μ, in GPa), universal anisotropy index (A^U) and the percentage of compression and shear anisotropy (A_K and A_μ, respectively) calculated according to the Voigt (V), Reuss (R) and Voigth-Reuss-Hill (VRH) formulas (see text for details).

Method	K_V	K_R	K_{VRH}	μ_V	μ_R	μ_{VRH}	A^U	A_K	A_μ
LDA	100.32	87.82	94.07	41.29	29.23	35.26	2.20	6.64	17.09
PBE	80.39	73.96	77.17	36.39	29.34	32.87	1.29	4.17	10.73
PBE-D2	86.46	76.49	81.47	38.55	28.61	33.58	1.87	6.12	14.80
PBE-D3	86.43	78.41	82.42	37.98	29.36	33.67	1.57	4.87	12.80
M06L	95.37	83.84	89.60	39.05	26.44	32.75	2.52	6.43	19.25
M06L-D3	95.60	83.86	89.73	39.05	26.42	32.74	2.53	6.54	19.30
B3LYP	82.28	75.87	79.07	39.27	31.56	35.41	1.31	4.05	10.89
B3LYP-D*	87.05	79.15	83.10	40.00	30.48	35.24	1.66	4.75	13.51
B3LYP-D3	93.51	83.72	88.62	43.00	31.91	37.46	1.85	5.52	14.80
PBE0	85.21	78.26	81.73	39.37	31.15	35.26	1.41	4.25	11.66
PBE0-D2	91.77	80.82	86.29	41.57	29.73	35.65	2.13	6.34	16.62
PBE0-D3	91.25	82.65	86.95	40.94	30.84	35.89	1.74	4.94	14.07
M06	103.10	93.35	98.22	44.74	33.91	39.33	1.70	4.96	13.77
M06-D3	104.75	94.74	99.75	45.00	33.67	39.33	1.79	5.01	14.40
Exp. [12]	*79.3*	*72.9*	*76.1*	*37.4*	*31.3*	*34.3*	*1.06*	*4.20*	*8.88*
Exp. [52]	*76*	*70.6*	*73.3*	*36.8*	*23.9*	*30.3*	*2.78*	*3.68*	*21.25*
PBE [53]	*67.9*	*59.9*	*63.9*	*39.2*	*35.7*	*37.5*	*0.62*	*6.26*	*4.67*
FF [17]	*77.6*	*70.1*	*73.8*	*40.1*	*34.6*	*37.4*	*0.90*	*5.08*	*7.36*

Notes: Values in italic were calculated in the present work. FF stands for force field (classical mechanics).

Table 4.
Young's (E, in GPa) moduli and Poisson's ratio (υ, dimensionless) calculated according to the Voigt (V), Reuss (R) and Voigth-Reuss-Hill (VRH) formulas (see text for details).

Method	E_V	E_R	E_{VRH}	υ_V	υ_R	υ_{VRH}
LDA	108.91	78.94	94.03	0.319	0.350	0.333
PBE	94.86	77.75	86.34	0.303	0.325	0.314
PBE-D2	100.69	76.30	88.57	0.306	0.334	0.319
PBE-D3	99.39	78.30	88.91	0.308	0.334	0.320
M06L	103.09	71.78	87.57	0.320	0.357	0.337
M06L-D3	103.12	71.72	87.56	0.320	0.357	0.337
B3LYP	101.64	83.14	92.44	0.294	0.317	0.305
B3LYP-D*	104.07	81.03	92.63	0.301	0.329	0.314
B3LYP-D3	111.86	84.94	98.49	0.301	0.331	0.315
PBE0	102.36	82.51	92.49	0.300	0.324	0.311
PBE0-D2	108.36	79.44	94.01	0.303	0.336	0.318
PBE0-D3	106.85	82.29	94.66	0.305	0.334	0.319
M06	117.26	90.75	104.09	0.310	0.338	0.323
M06-D3	118.08	90.32	104.30	0.312	0.341	0.326
Exp. [12]	*97*	*82.1*	*89.6*	*0.296*	*0.312*	*0.304*
Exp. [52]	*95.1*	*64.4*	*80*	*0.292*	*0.348*	*0.318*
PBE [53]	*98.7*	*89.4*	*94.1*	*0.258*	*0.251*	*0.255*
FF [17]	*102.7*	*89.2*	*96*	*0.279*	*0.288*	*0.283*

Notes: Values in italic were calculated in the present work. FF stands for force field (classical mechanics).

approximation reducing the number of required simulations at the expense of quantitative accuracy. Their employment are beyond the scope of the present work, but they will be discussed in a future work with only some selected DFT functionals.

As expected, an increase of the calcite stiffness with the inclusion of dispersive interactions was observed (**Fig. 2**). The most affected elastic constants were the C_{1u} ones and $C_{66} = ½(C_{11} - C_{12})$, whereas the C_{33} elastic constant increased by a lower amount (up to about 4%). This suggests that there is an enhanced repulsive interaction between the carbonate ion groups lying on planes perpendicular to the [001] direction (*xy* plane in Cartesian coordinates). In general, an increase of the C_{vu} values may be desirable since the crystal system is at absolute 0 K and zero-point/thermal effects were not considered. However, some of the DFT functional/DFT-D*n* combinations results in a too stiff mineral phase when compared to the experiments.

By comparing the effects of DFT-*Dn* corrections within the same DFT functional, it can be noted that the two schemes increase the calcite stiffness, with the DFT-D2 approach resulting in higher values of the elastic constants with respect to the DFT-D3 one. For example, for the standard GGA functional the calcite stiffness follows the trend PBE-D2 < PBE-D3 < PBE, which is also the trend observed for the unit cell volume previously discussed in Section 3.1. The elastic constants obtained with the uncorrected PBE are in better agreement with the experimental findings than those calculated at PBE-D2 and PBE-D3 levels, whose values are generally overestimated up to about 15%. Also, the C_{vu} calculated with the hybrid functionals B3LYP and PBE0 are always overestimated (up to about 20%), with a trend that increases as B3LYP < B3LYP-D* < B3LYP-D3 and PBE0 < PBE-D2 ≈ PBE-D3.

As expected, the largest deviations were obtained from the local density approximation (LDA) functional, because of its overbinding effect. However, large differences were also observed for the M06L meta-GGA Hamiltonian and for its hybrid formulation M06, with M06L < M06. For these two functionals, the DFT-D3 scheme had a low influence on the elastic constants, in agreement with the structural results.

The results obtained with the PBE functional not corrected for weak interactions are the closest to the experimental data, but this is probably due to a cancellation of errors, *i.e.,* underbinding on one side, Pulay stress on the other. Ultimately, in view of all the considerations reported above, the elastic properties evaluated with the PBE-D*n*, B3LYP, B3LYP-D*, PBE0 and PBE0-D*n* combinations are the ones closer to the experimental results, considering all the approximations introduced in the simulations.

The present data are in line with those of one of the first theoretical investigation on the elastic properties of calcite, conducted by Pavese and collaborators more than twenty years ago [17]. They employed a force field (FF) approach with a potential labelled as MS, where a Morse potential was used to describe the covalent C–O bonds, whereas Ca–O and O–O were modelled as Born-type interactions, including a shell model for the oxygen atom. This work was also one of the first where the thermal effects on structural and mechanical properties were included through the well-known quasi-harmonic approximation. Unfortunately, the authors did not report elastic constants calculated at 0 K, hence it is not straightforward comparing the semi-empirical and *ab initio* results.

However, compared to the more recent quantum mechanical results of Brik [53], our simulations evinced a substantial improvement of the elastic properties. In fact, several stiffness values reported in the cited work are underestimated, such as the C_{33} value that is about –20% the experimental ones [12,13,52]. Surprisingly, it was reported a zero value for the C_{14} modulus, because the author performed the simulations using an hexagonal lattice. To be remembered that calcite belongs instead to the trigonal crystal system, with a rhombohedral primitive cell. While this discrepancy does not influence the polycrystalline averages, as C_{14} does not enter in any of the expressions reported in the Computational Methods section (see Tables 3 and 4), it deeply affects the single-crystal directional elastic properties. This is graphically shown in Fig. 3, where the directional variations of the Young's and shear moduli, linear compressibility and Poisson's ratio were calculated and plotted using the results of Brik (blue line) [53].

The elastic anisotropy of calcite can be also described by the universal anisotropic index, A^U, as described by Ranganathan and Ostoja-Starzewski [57]. This term is calculated from the ratio of the bulk and shear moduli according to the following expression:

$$A^U = 5\frac{\mu_V}{\mu_R} + \frac{K_V}{K_R} - 6 \geq 0$$

with K_V, K_R, μ_V and μ_R the Voigt and Reuss bounds of the bulk and shear moduli, respectively. For isotropic media, the ratio between the Voigt and Reuss moduli is equal to unity, hence the $A^U = 0$, whereas the universal anisotropy index is greater than zero when the crystal exhibits mechanical anisotropy. The percent anisotropy in compression (A_K) and shear (A_μ) can be expressed as:

$$A_K = 100\frac{K_V - K_R}{K_V + K_R} \text{ and } A_\mu = 100\frac{\mu_V - \mu_R}{\mu_V + \mu_R}$$

The anisotropy results are reported in Table 3, showing that the A^U values calculated with the different DFT approaches are between those experimentally evaluated (1.06 – 2.78) [12,52]. The same applies to the percentage of shear anisotropy, A_μ (8.88% – 21.25% at experimental level), but the theoretical values of the A_K index are generally greater than the experimental range of 3.68% – 4.20%. The present A^U and A_μ indexes are greater than those from previous theoretical DFT/PBE [53] and force field simulations [17], which were underestimated with respect to the experimental data. However, the percentage of compression anisotropy is similar between the different approaches. This means that the present DFT methods are consistent and able to provide an adequate description of the anisotropic elastic behaviour of calcite.

3.2.2. *Equation of state*

To calculate the equation of state of calcite, *i.e.*, to provide a description of how the unit cell volume varies with hydrostatic pressure, it was employed the phenomenological third-order Birch-Murnaghan (BM3) formulation [58]. In details, six unit cell volumes between $0.96V_{eq}$ and $1.06V_{eq}$ (V_{eq} is the equilibrium geometry previously calculated) were modelled and their geometry optimized at constant volume, to simulate the effect of positive/negative hydrostatic pressure acting on the mineral [59]. The equation of state was then calculated from energy E versus volume V curves, according to a volume-integrated BM3 formulation, as proposed by Hebbache and Zemzemi [60]:

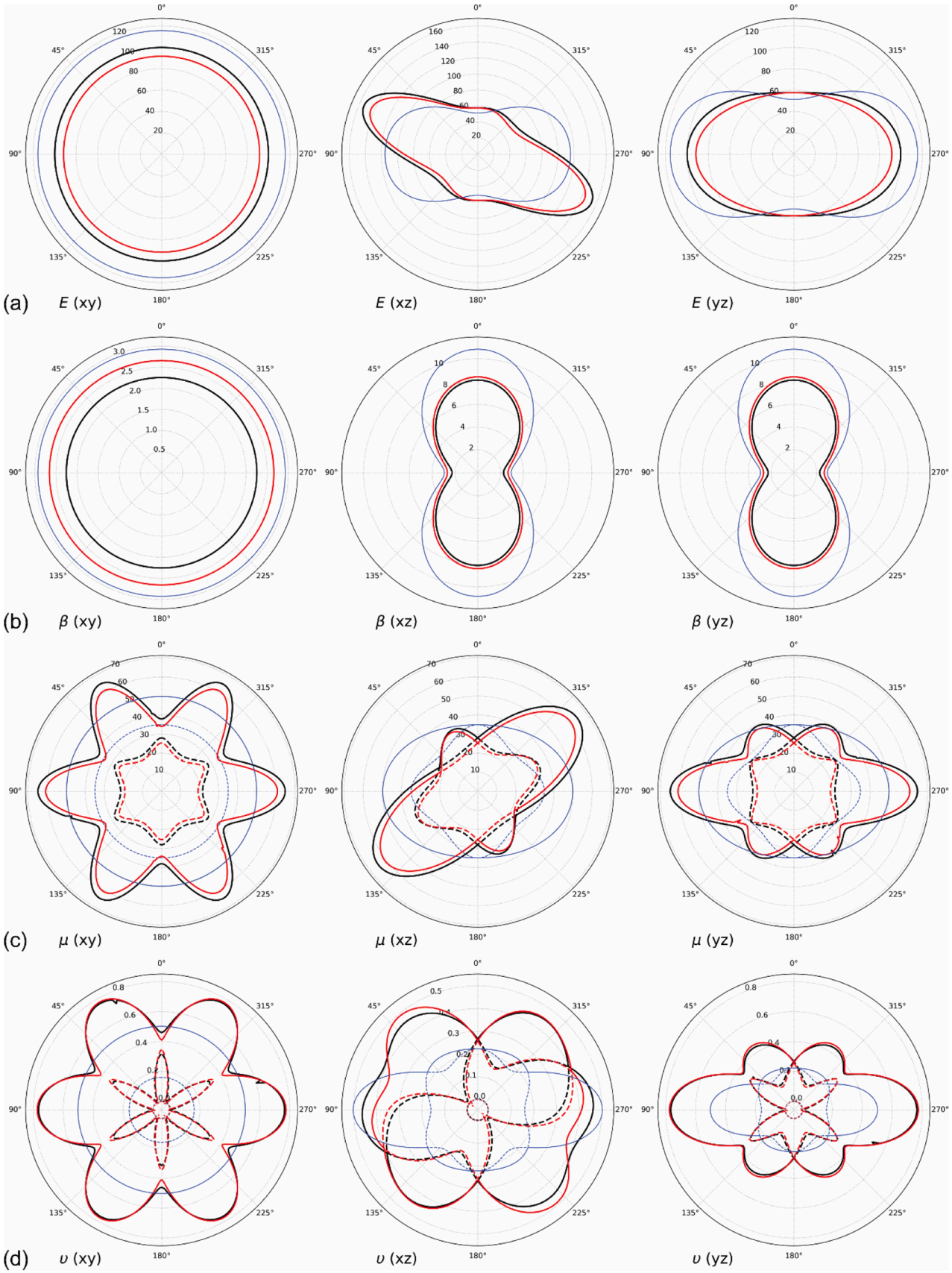

Fig. 3. Spatial dependence of (a) Young's modulus E, (b) linear compressibility β, (c) shear modulus μ and (d) Poisson's ratio υ on the (xy), (xz) and (yz) planes. Black lines are related to our B3LYP-D* results, the red lines are from the experimental data of Chen and co-workers[12] and the blue lines where calculated from the theoretical data of Brik.[53] In (c) and (d), solid and dashed lines are referred to the maximum and minimum values, respectively, of the elastic properties. (For interpretation of the references to color in this figure legend, the reader is referred to the web version of this article.)

$$E(V) = E_0 + \frac{9}{16}K_0V_0\left\{K';(X^2-1)^3 + \left[(X^2-1)^2(6-4X^2)\right]\right\}$$

where the fitting parameters are the unit cell energy E_0, the bulk modulus K_0, the pressure first derivative of the bulk modulus K' and the unit cell volume V_0, each referred at 0 GPa. The term $X = (V_0/V)^{-1/3}$ was introduced to ease the readability. The results of the equation of state fitting are reported in Table 5, considering the crystallographic trigonal cell.

The calculated K_0 values obtained with each method differs no more than 1.3% than the K_R (Reuss bound) data obtained from the elastic moduli (see Table 3). The same applies to the calculated V_0 volumes, which are very close to the equilibrium ones (maximum difference of 0.05%). These results indicate the consistency between the equation of state and the elastic constants calculations, which is an important assessment of the quality of the simulation approach. All the methods showed a variation of the bulk modulus with pressure $K' \approx 4$, indicating that a second-order Birch-Murnaghan formulation could be sufficient to describe the elastic behaviour of the mineral under hydrostatic compression. The only exception is given by the M06L and M06L-D3 approaches, whose very low pressure first-derivative of the bulk modulus K' suggests a very stiff behaviour of the mineral.

The theoretical results are in good agreement with the experimental high-pressure analysis performed by Redfern and Angel on a single crystal of calcite at room temperature (298 K) [15]. The authors employed a second-order Birch-Murnaghan equation of state to fit the pressure versus volume crystallographic data. As previously discussed, the slightly stiffer behaviour of the mineral from the DFT simulations is expected because the *ab initio* simulations are at 0 K and without any thermal contribution. The PBE results are very close to the experimental one, and it is suspected that the eventual inclusion of thermal effects would result in a softer behaviour with respect to the experimental evidence. Conversely, the DFT-D3 scheme applied to B3LYP and PBE0 resulted in a very high K_0 value. Among the different approaches here considered, the hybrid M06 and M06-D3 produced the stiffest behaviour of the calcite unit cell under hydrostatic compression, followed by LDA, in agreement with the analysis of the second-order elastic constants. There is also an agreement with a theoretical investigation conducted on the thermodynamic and thermoelastic properties of calcite, performed with the CRYSTAL code using the hybrid WC1LYP functional and Gaussian-type basis sets [18]. Unfortunately, the authors did not report the static (0 K) bulk modulus of calcite for a direct comparison between the different approaches here employed.

Until now, it was not considered including a proper treatment for the long-range interactions in the DFT simulations of calcite, an anisotropic and heterodesmic material. Previous theoretical works showed that standard DFT functionals (*e.g.*, PBE, B3LYP) overestimates the lattice parameters and structure-dependent properties [16,61]. Global hybrid functionals, such as B3LYP and PBE0, usually increase the ionic character of solids because of the augmented electron localization due to the fraction of Hartree-Fock exact exchange. As also discussed elsewhere [62], it is a cancellation of two effects with opposite signs: on one side, GGA functionals lead to different degrees of underbinding, on the other side Hartree-Fock does the opposite. The small discrepancies observed with the B3LYP and PBE0 hybrid functionals could be indeed reduced by employing the proposed schemes to include van der Waals interactions. Indeed, tt was recently shown that the inclusion of long-range interactions could play an important role in determining the structural, vibrational and thermoelastic properties of stoichiometric and carbonated hydroxylapatite, which is another anisotropic and heterodesmic mineral phase [63–66]. Alternatively, it could be devised the use of the so-called 'self-consistent hybrids', *i.e.*, hybrid Hamiltonians whose exact exchange fraction is recalculated by iterative procedures on some selected properties, such as the dielectric response [67]. This approach could ameliorate the results obtained with the M06 hybrid functional, which resulted in a too stiff behaviour, even at absolute zero.

However, for Hamiltonians based on the generalized gradient approximation and the use of a DFT-D*n* correction scheme seems ameliorating the description of the calcite system. Since hybrid functionals may be very expensive depending on the computational settings, *e.g.*, they are still prohibitive for most systems using plane waves basis sets, because the *a posteriori* inclusion of weak dispersive forces in the physical treatment could be a suitable way to improve the quality of the simulations.

Finally, the authors are aware that there are other approaches to include the long-range interactions in the DFT simulations, both within the DFT framework, *e.g.*, the vdW-DF non-local correlation functional proposed by Dion and co-workers [68], and as *a posteriori* corrections schemes, such as the Tkatchenko-Scheffler method [69]. They were not tested at the moment because they have not been implemented in the CRYSTAL code, but it is planned a future work on this topic when they will be available.

4. Conclusions

Calcite is an important and ubiquitous mineral that belongs to the

Table 5.
Third-order Birch-Murnaghan equation of state parameters K_0 (GPa), K' and V_0 (Å^3), calculated with different DFT approaches, compared to previous theoretical and experimental results. Equilibrium volume, V_{eq} (Å^3), and the bulk modulus calculated at the Reuss bound, K_R (GPa) were reported for the sake of comparison. ΔV and ΔK are the relative differences (%) between V_0 and V_{eq}, and K_0 and K_R, respectively.

Method	K_0	K'	V_0	V_{eq}	ΔV	K_R	ΔK
LDA	87.83(5)	3.88(6)	350.827(11)	350.86	–0.01	87.82	0.01
PBE	73.56(3)	4.30(4)	381.767(9)	381.67	0.03	73.96	–0.54
PBE-D2	76.01(6)	4.22(7)	370.127(9)	370.08	0.01	76.49	–0.63
PBE-D3	77.40(3)	4.15(4)	372.689(7)	372.64	0.01	78.41	–1.29
M06L	83.0(1)	1.74(16)	369.246(29)	369.23	0.00	83.84	–1.00
M06L-D3	82.8(2)	1.76(17)	367.947(35)	367.93	0.00	83.86	–1.26
B3LYP	75.70(2)	4.42(4)	381.267(8)	381.08	0.05	75.87	–0.22
B3LYP-D*	78.40(3)	4.28(4)	371.684(8)	371.52	0.04	79.15	–0.95
B3LYP-D3	83.07(3)	3.97(3)	371.684(8)	365.17	1.78	83.72	–0.78
PBE0	77.75(5)	4.25(6)	373.940(11)	373.73	0.06	78.26	–0.65
PBE0-D2	80.37(2)	3.98(2)	362.580(4)	362.42	0.04	80.82	–0.56
PBE0-D3	81.99(7)	4.03(9)	365.010(16)	364.85	0.04	82.65	–0.80
M06	91.9(2)	4.7(3)	365.417(48)	365.30	0.03	93.35	–1.55
M06-D3	93.11(3)	4.7(3)	363.748(52)	363.63	0.03	94.74	–1.72
W1CLYP [a] [18]	75.58	-	-	-	-	-	-
Experimental [15],[b]	73.46(27)	4	122.596(4)	-	-	-	-

[a] Calculated at 298 K;
[b] Experimental data fitted to a second-order Birch-Murnaghan equation of state, where K' is fixed at 4. Values in parentheses are the errors associated to the fitting procedure.

trigonal crystal system ($CaCO_3$ space group $R\bar{3}c$) and, because of its heterodesmic, composite-like crystal structure, presents anisotropic physical properties that can be exploited in various basic and applicative fields. Among them, the elastic properties were the focus of the present work because they are important for the employment of this mineral in composites and buildings and construction materials. In addition, since many physical properties of calcite, including elasticity, are well-known in literature, this crystal phase is suitable as a model to evaluate the effectiveness of theoretical simulation methods in obtaining, and eventually predicting, the desired properties of anisotropic and heterodesmic materials.

The backbone of the theoretical simulations here presented is given by the Density Functional Theory, employing Gaussian-type orbitals basis sets to describe the atoms. The structural and elastic (stiffness and equation of state) results were obtained from fourteen combinations between six DFT functionals of different complexity (LDA, PBE, M06L, PBE0, B3LYP and M06) and *a posteriori* corrections to include long-range interactions (DFT-D2 and DFT-D3). In the present work, they were compared and discussed with each other and constructively related to the experimental data reported in literature. In conclusion, and considering the static limit of the present work that was conducted 0 K, with no thermal effects), we can summarize:

- the calcite structure (lattice parameters and internal geometry) was well described by the hybrid functionals PBE0 and B3LYP corrected for the van der Waals interactions (PBE0-D3 and B3LYP-D*);
- a correction to include the long-range interactions in the physical treatment can be mandatory when employing standard generalized-gradient approximation functionals and their hybrid counterparts. For calcite, it greatly improved the c/a ratio, C–O bonds and Ca—O interaction distances, for PBE (the most affected), B3LYP and PBE0. Conversely, when using M06L and M06, the DFT-D3 correction scheme did not provide much different results in comparison with the uncorrected functionals. Since the parameters for this correction scheme are recalculated according to the geometry of the system under consideration, this result suggests that the Laplacian (second-derivative) of the electron density included in the meta-GGA functional is able to better describe the bonds and long-range interactions between atoms, with respect to the local density and generalized-gradient approximations;
- the elastic moduli of calcite are generally overestimated with respect to the experimental results because of the Pulay stress and the absence of thermal effects. It was observed an inverse proportionality between the calculated unit cell volume and the mineral stiffness, with the best results provided by the B3LYP-D* and PBE0-D3 approaches corrected for long-range interactions. The LDA and meta-GGA resulted in a too high stiffness of calcite with respect to the experimental data, with bulk moduli K_{VRH} overestimated up to about 30%, just to cite an example.

The present work shows that the choice of the computational parameters for the simulations is relevant to obtain consistent and reliable results. Such choice is of utmost importance when characterizing the physical and chemical properties of less known materials, and even more when designing new, innovative ones. Here, the aim was providing a benchmark between different DFT approaches in the description of the structure and elasticity of calcite, the latter being often overlooked in favour of other properties, to help theoretical researchers in devising their simulations for similar heterodesmic crystal structures.

In future, the present approach will be extended by including thermal effects on the calculated properties, to obtain a complete calibration of the structural and elastic properties of calcite at different temperature and pressure conditions. Furthermore, other DFT functionals, some of them including an *ad hoc* contribution of van der Waals interactions (for example the vdW-DF functional), and other computational parameters, such as basis sets (*e.g.*, numeric atomic orbitals, planewaves), will be included.

Data availability

The data are available within the present work.

Funding

The present work did not receive any specific funding.

Declaration of competing interest

The authors declare that they have no known competing financial interests or personal relationships that could have appeared to influence the work reported in this paper.

References

[1] MI. Petrescu, Boron nitride theoretical hardness compared to carbon polymorphs, Diamond Relat. Mater. 13 (2004) 1848–1853.
[2] G Ulian, S Tosoni, G. Valdrè, The compressional behaviour and the mechanical properties of talc [$Mg_3Si_4O_{10}(OH)_2$]: a density functional theory investigation, Phys. Chem. Miner. 41 (2014) 639–650.
[3] G Ulian, G. Valdrè, Equation of state and second-order elastic constants of portlandite $Ca(OH)_2$ and brucite $Mg(OH)_2$, Phys. Chem. Miner. 46 (2019) 101–117.
[4] G Ulian, D Moro, G. Valdrè, Electronic and optical properties of graphene/molybdenite bilayer composite, Compos. Struct. (2021) 255.
[5] GH. Davis, Stylolitic limestone, the stone of choice for ancient sanctuaries and temples, southwestern Peloponnese, Greece, Geoarchaeology. 33 (2018) 708–722.
[6] L Maritan, G Ganzarolli, F Antonelli, M Rigo, A Kapatza, K Bajnok, et al., What kind of calcite? Disclosing the origin of sparry calcite temper in ancient ceramics, J. Archaeol. Sci. (2021) 129.
[7] G Scardozzi, M Brilli, F. Giustini, Calcite alabaster artifacts from Hierapolis in Phrygia, Turkey: provenance determination using carbon and oxygen stable isotopes, Geoarchaeology 34 (2019) 169–186.
[8] R. Siddall, The Use of Volcaniclastic Material in Roman Hydraulic Concretes: A Brief Review, Geological Society Special Publication, 2000, pp. 339–344.
[9] Y Dhandapani, M Santhanam, G Kaladharan, S. Ramanathan, Towards ternary binders involving limestone additions — a review, Cement Concr. Res. (2021) 143.
[10] E Ermilova, Z Kamalova, R. Ravil, Influence of Clay Mineral Composition on Properties of Blended Portland Cement with Complex Additives of Clays and Carbonates, 1 ed, Institute of Physics Publishing, 2020.
[11] PE. Stutzman, Microscopy of clinker and hydraulic cements, Rev. Mineral. Geochem. (2012) 101–146.
[12] CC Chen, CC Lin, LG Liu, SV Sinogeikin, JD. Bass, Elasticity of single-crystal calcite and rhodochrosite by Brillouin spectroscopy, Am. Miner. 86 (2001) 1525–1529.
[13] DP. Dandekar, Variation in the elastic constants of calcite with temperature, J. Appl. Phys. 39 (1968) 3694–3699.
[14] DP. Dandekar, Elastic constants of calcite, J. Appl. Phys. 39 (1968) 2971–2973.
[15] SAT Redfern, RJ. Angel, High-pressure behaviour and equation of state of calcite, $CaCO_3$, Contrib. Mineral. Petrol. 134 (1999) 102–106.
[16] L Valenzano, FJ Torres, D Klaus, F Pascale, CM Zicovich-Wilson, R Dovesi, Ab initio study of the vibrational spectrum and related properties of crystalline compounds; the case of $CaCO_3$ calcite, Zeitschrift Fur Physikalische Chemie - Int. J. Res. Phy. Chem. Chem. Phys. 220 (2006) 893–912.
[17] A Pavese, M Catti, SC Parker, A. Wall, Modelling of the thermal dependence of structural and elastic properties of calcite, $CaCO_3$, Phys. Chem. Miner. 23 (1996) 89–93.
[18] CG Ungureanu, R Cossio, M. Prencipe, An ab-initio assessment of thermo-elastic properties of $CaCO_3$ polymorphs: Calcite case, CALPHAD: Comput. Coupling Phase Diagrams Thermochem. 37 (2012) 25–33.
[19] R Demichelis, B Civalleri, M Ferrabone, R Dovesi, On the performance of eleven DFT functionals in the description of the vibrational properties of aluminosilicates, Int. J. Quant. Chem. 110 (2010) 406–415.
[20] P Hao, J Sun, B Xiao, A Ruzsinszky, GI Csonka, J Tao, et al., Performance of meta-GGA functionals on general main group thermochemistry, kinetics, and noncovalent interactions, J. Chem. Theory Comput. 9 (2013) 355–363.
[21] G Ulian, D Moro, G. Valdrè, Benchmarking dispersion-corrected DFT methods for the evaluation of materials with anisotropic properties: calcite ($CaCO_3$, space group *R*-3*c*) as test case, Phys. Chem. Chem. Phys. (2021), https://doi.org/10.1039/D1CP02673A.
[22] R Dovesi, A Erba, R Orlando, CM Zicovich-Wilson, B Civalleri, L Maschio, et al., Quantum-mechanical condensed matter simulations with CRYSTAL, Wiley Interdiscip. Rev.-Comput. Mol. Sci. 8 (2018) E1360.
[23] B Xiao, J Sun, A Ruzsinszky, JP. Perdew, Testing the Jacob's ladder of density functionals for electronic structure and magnetism of rutile VO_2, Phys. Rev. B (2014) 90.
[24] JP Perdew, K Burke, M. Ernzerhof, Generalized gradient approximation made simple, Phys. Rev. Lett. 77 (1996) 3865–3868.

[25] Y Zhao, DG. Truhlar, The M06 suite of density functionals for main group thermochemistry, thermochemical kinetics, noncovalent interactions, excited states, and transition elements: two new functionals and systematic testing of four M06-class functionals and 12 other functionals, Theor. Chem. Acc. 120 (2008) 215–241.
[26] AD. Becke, A new mixing of hartree-fock and local density-functional theories, J. Chem. Phys. 98 (1993) 1372–1377.
[27] CT Lee, WT Yang, RG. Parr, Development of the Colle-Salvetti correlation-energy formula into a functional of the electron-density, Phys. Rev. B 37 (1988) 785–789.
[28] HJ Monkhorst, JD. Pack, Special points for Brillouin-zone integrations, Phys. Rev. B 8 (1976) 5188–5192.
[29] L Valenzano, Y Noel, R Orlando, CM Zicovich-Wilson, M Ferrero, R. Dovesi, Ab initio vibrational spectra and dielectric properties of carbonates: magnesite, calcite and dolomite, Theor. Chem. Acc. 117 (2007) 991–1000.
[30] A Ruzsinszky, JP Perdew, GI. Csonka, Binding energy curves from nonempirical density functionals II. van der Waals bonds in rare-gas and alkaline-earth diatomics, J. Phys. Chem. A 109 (2005) 11015–11021.
[31] A Ruzsinszky, JP Perdew, GI. Csonka, Binding energy curves from nonempirical density functionals. I. Covalent bonds in closed-shell and radical molecules, J. Phys. Chem. A 109 (2005) 11006–11014.
[32] J Tao, JP Perdew, A. Ruzsinszky, Accurate van der Waals coefficients from density functional theory, Proc. Natl. Acad. Sci. U. S. A. 109 (2012) 18–21.
[33] S. Grimme, Semiempirical GGA-type density functional constructed with a long-range dispersion correction, J. Comput. Chem. 27 (2006) 1787–1799.
[34] S Grimme, S Ehrlich, L. Goerigk, Effect of the damping function in dispersion corrected density functional theory, J. Comput. Chem. 32 (2011) 1456–1465.
[35] AD Becke, ER. Johnson, A density-functional model of the dispersion interaction, J. Chem. Phys. (2005) 123.
[36] ER Johnson, AD. Becke, A post-Hartree-Fock model of intermolecular interactions, J. Chem. Phys. (2005) 123.
[37] ER Johnson, AD. Becke, A post-Hartree-Fock model of intermolecular interactions: Inclusion of higher-order corrections, J. Chem. Phys. 124 (2006).
[38] JF. Nye, Physical Properties of Crystals, Oxford University Press, Oxford, 1957.
[39] WF. Perger, First-principles calculation of second-order elastic constants and equations of state for lithium azide, LiN_3, and lead azide, $Pb(N_3)_2$, Int. J. Quant. Chem. 110 (2010) 1916–1922.
[40] WF Perger, J Criswell, B Civalleri, R. Dovesi, Ab-initio calculation of elastic constants of crystalline systems with the CRYSTAL code, Comput. Phys. Commun. 180 (2009) 1753–1759.
[41] JG. Brainerd, Standards on piezoelectric crystals, Proc. IRE 37 (1949) 1378–1395.
[42] Ulian G, Valdrè G. QUANTAS, a Python software for the analysis of solids from ab initio quantum mechanical simulations and experimental data. 2021;in preparation.
[43] A Marmier, ZAD Lethbridge, RI Walton, CW Smith, SC Parker, KE. Evans, ElAM: A computer program for the analysis and representation of anisotropic elastic properties, Comput. Phys. Commun. 181 (2010) 2102–2115.
[44] R Gaillac, P Pullumbi, FX. Coudert, ELATE: an open-source online application for analysis and visualization of elastic tensors, J. Phys.: Condens. Matter 28 (2016), 275201.
[45] G Ulian, D Moro, G. Valdrè, First principle investigation of the mechanical properties of natural layered nanocomposite: Clinochlore as a model system for heterodesmic structures, Compos. Struct. 202 (2018) 551–558.
[46] R. Hill, The elastic behaviour of a crystalline aggregate, Proc. Phys. Soc. Lond. Sec. A 65 (1952) 349–354.
[47] EN Maslen, VA Streltsov, NR. Streltsova, X-ray study of the electron-density in calcite, $CaCO_3$, Acta Crystallogr. Sec. B-Struct. Sci. 49 (1993) 636–641.
[48] M Corno, C Busco, B Civalleri, P. Ugliengo, Periodic ab initio study of structural and vibrational features of hexagonal hydroxyapatite $Ca_{10}(PO_4)_6(OH)_2$, Phys. Chem. Chem. Phys. 8 (2006) 2464–2472.
[49] G Ulian, G. Valdrè, Second-order elastic constants of hexagonal hydroxylapatite ($P6_3$) from ab initio quantum mechanics: comparison between DFT functionals and basis sets, Int. J. Quant. Chem. 118 (2018).
[50] B Civalleri, CM Zicovich-Wilson, L Valenzano, P. Ugliengo, B3LYP augmented with an empirical dispersion term (B3LYP-D*) as applied to molecular crystals, CrystEngComm 10 (2008) 405–410.
[51] G Ulian, S Tosoni, G. Valdrè, Comparison between Gaussian-type orbitals and plane wave ab initio density functional theory modeling of layer silicates: talc $Mg_3Si_4O_{10}(OH)_2$ as model system, J. Chem. Phys. (2013) 139.
[52] RFS. Hearmon, The elastic constants of crystals and other anisotropic materials, in: KH Hellwege, AM Hellwege (Eds.), Landolt-Bornstein Tables, Springer-Verlag, Berlin, Germany, 1979.
[53] MG. Brik, First-principles calculations of structural, electronic, optical and elastic properties of magnesite $MgCO_3$ and calcite $CaCO_3$, Physica B 406 (2011) 1004–1012.
[54] GP Francis, MC. Payne, Finite basis set corrections to total energy pseudopotential calculations, J. Phys.: Condens. Matter 2 (1990) 4395–4404.
[55] G Ulian, G. Valdre, Equation of state of hexagonal hydroxylapatite (P6(3)) as obtained from density functional theory simulations, Int. J. Quant. Chem. 118 (2018) e25553.
[56] M Destefanis, C Ravoux, A Cossard, A. Erba, Thermo-elasticity of materials from quasi-harmonic calculations, Minerals 9 (2019).
[57] SI Ranganathan, M. Ostoja-Starzewski, Universal elastic anisotropy index, Phys. Rev. Lett. 101 (2008), 055504.
[58] F. Birch, Finite elastic strain of cubic crystal, Phys. Rev. 71 (1947) 809–824.
[59] A Erba, A Mahmoud, D Belmonte, R. Dovesi, High pressure elastic properties of minerals from ab initio simulations: The case of pyrope, grossular and andradite silicate garnets, J. Chem. Phys. 140 (2014), 124703.
[60] M Hebbache, M. Zemzemi, Ab initio study of high-pressure behavior of a low compressibility metal and a hard material: Osmium and diamond, Phys. Rev. B (2004) 70.
[61] M Prencipe, F Pascale, CM Zicovich-Wilson, VR Saunders, R Orlando, R. Dovesi, The vibrational spectrum of calcite ($CaCO_3$): an ab initio quantum-mechanical calculation, Phys. Chem. Miner. 31 (2004) 559–564.
[62] F Cora, M Alfredsson, G Mallia, DS Middlemiss, WC Mackrodt, R Dovesi, et al., The performance of hybrid density functionals in solid state chemistry, in: N Kaltsoyannis, JE McGrady (Eds.), Principles and Applications of Density in Inorganic Chemistry Ii, Springer-Verlag Berlin, Berlin, 2004, pp. 171–232.
[63] G Ulian, D Moro, G. Valdrè, Thermodynamic, elastic and vibrational (IR/Raman) behaviour of mixed type-AB carbonated hydroxylapatite by density functional theory, Am. Mineral. (2021). Accepted.
[64] G Ulian, G. Valdrè, Equation of state of hexagonal hydroxylapatite (P6(3)) as obtained from density functional theory simulations, Int. J. Quant. Chem. 118 (2018).
[65] G Ulian, G. Valdrè, First principle investigation of the thermomechanical properties of type A carbonated apatite, Int. J. Quant. Chem. (2019) 120.
[66] G Ulian, G. Valdrè, Thermodynamic and thermoelastic data of georesources raw minerals: Zinc sulphide and apatite, Data Brief 29 (2020).
[67] JH Skone, M Govoni, G. Galli, Self-consistent hybrid functional for condensed systems, Phys. Rev. B 89 (2014), 195112.
[68] M Dion, H Rydberg, E Schröder, DC Langreth, BI. Lundqvist, Van der Waals Density Functional for General Geometries, Phys. Rev. Lett. 92 (2004), 246401.
[69] A Tkatchenko, M. Scheffler, Accurate molecular van der Waals interactions from ground-state electron density and free-atom reference data, Phys. Rev. Lett. 102 (2009), 073005.